Fuel 262 (2020) 116596

Contents lists available at ScienceDirect

Fuel

journal homepage: www.elsevier.com/locate/fuel

Full Length Article

Experimental study on the combustion characteristics of high-pressure octanal spray flames

Irene Ruiz-Rodriguez[a,*], Roger Cracknell[b], Michael Parkes[b], Thanos Megaritis[a], Lionel Ganippa[a]

[a] Mechanical, Aerospace and Civil Engineering Department, Brunel University London, UB8 3PH, United Kingdom
[b] Shell Global Solutions UK, 40 Bank Street, Canary Wharf, London E14 5NR, United Kingdom

ARTICLE INFO

Keywords:
Oxygenated fuels
Octanal
C8 fuel
Two-colour pyrometry
Diesel combustion
Soot

ABSTRACT

In view of the stringent emission regulations, oxygenated fuels are growing in popularity owing to their potential to reduce emissions in diesel vehicles and off-road applications. It is important to explore the combustion characteristics of oxygenates that can match the energy content and density of diesel whilst reducing the formation of pollutants. Furthermore, having similar thermo-physical properties to diesel could yield them as drop-in fuel candidates. In this work, the combustion characteristics of a long carbon chain oxygenate, octanal ($C_8H_{16}O$), and diesel, were investigated using the two-colour pyrometry method to study the temperature and soot distributions in the spray flames. This investigation was done by injecting the fuels at high pressures in an optically accessible constant volume chamber under a diesel engine-like environment, at high ambient pressures and temperatures. The soot lift-off length for octanal was longer than for diesel, which reduced the amount of time available for soot to grow. For the same injected mass of diesel and octanal, the combustion of octanal was faster due to the presence of fuel-bound oxygen. The two-colour pyrometry results revealed that the spatial distribution of soot for octanal was slightly different from that of diesel. The chemical structure of octanal, consisting of a long chain alkane with an aldehyde functional group at the end and without the presence of any aromatic structures, hindered the soot formation significantly throughout the combustion process when compared to diesel.

1. Introduction

Diesel engines are widely used in transportation, power generation, off-road and agricultural applications because of their high thermal efficiency, reliability, and low maintenance costs. Despite their advantages, soot and NO_x emitted from diesel engines are of concern [1,2]. Furthermore, the production of soot indicates that the cycle is not as efficient as it could be. Efficiency losses due to soot formation can be attributed to radiation, and can amount up to 0.5%-10% of the total chemical energy released, depending on engine operating parameters [3,4]. Furthermore, clogging of diesel particulate filters (DPF) can increase fuel consumption by up to 4% [5]. Extensive research has shown that soot formation is partly dependent on fuel structure and is controlled by reaction kinetics during the early inception stages [6–8].

A promising strategy to reduce engine-out soot emissions is to reduce the formation rate and enhance the oxidation rate during combustion, by optimising fuel design [9–12]. Enhancing soot oxidation also has the additional benefit of enhancing engine efficiency, by speeding up the late combustion stages [13]. Recent works have shown that fuels with bound oxygen, known as oxygenated fuels, can reduce the production of soot during the combustion process by altering the local equivalence ratios [12,14–17]. Previous studies have made use of engines, constant volume chambers and laboratory flames to characterise the combustion of different short chain oxygenated fuels as blends with diesel or as neat fuels such as: dimethyl ether (DME), oxymethylene ether (OME), methyl decanoate, ethanol, methanol, butanol, propanol and furans [10,18,19]. Whilst understanding how a fuel would behave as a blend with diesel or as a drop-in fuel is key for the fuel design process, it is also important to understand the combustion characteristics of potential fuels neat, and to explore their performance and pollution properties independently of any base fuels. To date, the combustion of lower carbon-chain (C-chain) oxygenates has been widely researched, but very little information is available on higher C-chain oxygenates. The latter match the energetic properties of diesel better, and if they also have similar thermo-physical properties they could potentially serve as drop-in fuels or as replacements in current internal combustion engines (ICEs). Recent works on C4-C6 fuels suggest that the oxygenated compounds reduce soot production [20–22],

* Corresponding author.
E-mail address: irene.ruizrodriguez@brunel.ac.uk (I. Ruiz-Rodriguez).

https://doi.org/10.1016/j.fuel.2019.116596
Received 8 May 2019; Received in revised form 29 October 2019; Accepted 5 November 2019
Available online 18 November 2019

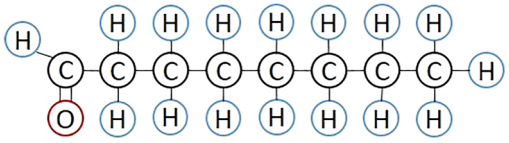

Fig. 1. Chemical structure of octanal.

and more recently, the works on the combustion characteristics in diesel engines of C8 oxygenated fuels such as di-n-butyl ether (DNBE) and 1-octanol have shown a cleaner combustion with low soot and low nitrogen oxide emissions [16,23]. Whilst their results show promising outcomes, more work is required to expand the database of knowledge on oxygenated fuels and to further our understanding of their combustion characteristics. It has been shown in [20,24,25] that short chain aldehydes have significant soot reduction properties, and hence they have the potential to be components in blends for future low emission fuels. An example of a higher C–chain aldehyde is octanal. The thermo-physical properties of octanal ($C_8H_{16}O$) (Fig. 1) and diesel, obtained from various sources, are shown in Table 1.

As seen in Table 1, octanal and diesel have a similar density and calorific value. Octanal has also been reported to have a low-toxicity [26], which makes it a viable fuel in terms of user-handling and transportation. It is noted that for general usage, octanal would be used as a drop-in fuel, which reduces the risks involved in end-user handling. Octanal can be produced by dehydrogenation of octanol using copper and magnesium oxide catalysts [27,28], which in turn can be produced from the biomass-derived molecules furfural and acetone [29]. Its production from initial biomass could also be advantageous from a greenhouse gas lifecycle assessment, as overall, biomass-based production methods have shorter carbon cycle systems [30]. Other octanal production pathways have been suggested in recent studies, which have proposed the synthesis of aldehydes via microbial engineering [31].

Based on its chemical structure, octanal could be a less polluting alternative fuel, however, no previous studies have investigated its combustion behaviour. To be able to determine its suitability as an alternative fuel, careful characterisation of its combustion properties is required. To this end, this study explores: the potential of using octanal as an alternative fuel under diesel engine-like operating conditions; the start and end of combustion properties of octanal (relative to its flame luminosity); the spatial soot distribution of octanal during the start of combustion, quasi-steady burn, and the end of combustion; and finally, its sooting tendency. The two-colour pyrometry method was used, and the data for octanal was systematically compared to the data for diesel obtained under the same ambient conditions.

2. Experiments and data analysis

2.1. Set-up and operating conditions

Investigations were conducted in a high-pressure, high-temperature constant volume chamber (CVC) with optical access that allowed for visualisation of the injected fuel. To achieve engine-like ambient conditions, the CVC was chemically pre-heated by combusting a lean mixture of C_2H_2 and air, which generated a high-temperature environment with ≈10% unburnt oxygen available for the main combustion of octanal and diesel. The unburned oxygen was determined by balancing the chemical equation for stoichiometry for C_2H_2 and air. By computing the required molar ratios to obtain the desired amount of unburned oxygen, one can use Dalton's laws to obtain the required partial pressures of the reactants. A separate study was conducted to verify the repeatability of the ambient conditions, where 15 pre-heating cycles were characterised showing a repeatability of 98%.

The fuel was injected using a six-hole common rail diesel injector into an environment at an ambient pressure of 36 bar and an ambient temperature of ≈1300 K. This temperature is significantly above the autoignition temperature of both fuels (Table 1), which enhanced the ignition kinetics for both. Hence the pre-mixing time available before ignition takes place is minimised- ensuring that the results were predominantly dependent on the chemical effect of the fuel. Ten injection events were considered for each fuel, and the same amount of fuel mass was injected for diesel and octanal by changing the programmed injection timings (1.5 ms for diesel and 1.8 ms for octanal). It is well established in literature that at least five injection events are required to provide sufficient data for combustion analysis [36–39], therefore the ten injection events performed should suffice to provide a statistically significant average. The data was acquired using a high-speed CMOS camera at 18 kHz with an exposure time of 54.54 µs, with an imaging area of 768pixels^2 × 960pixels^2 and with each pixel corresponding to approximately 90 µm. To maximise the camera's resolution, only one of the six flames was considered, and the image was doubled using a beam splitter and a mirror to obtain two images of the same flame simultaneously on the CMOS detector. Two narrow band-pass filters centred at wavelengths of 543.5 nm (λ_1) and 670 nm (λ_2) with Full Width Half Maximum (FWHM) of 10 nm were placed in front of the camera to acquire wavelength-specific images. The schematic of the set-up used in this investigation is shown in Fig. 2.

2.2. Two-colour pyrometry

The two-colour (2C) pyrometry method was used to determine the soot temperature, T, and the soot concentration in terms of the KL factor [40]. The 2C method is based on Planck's law of radiation for a blackbody, whose intensity (I_B) at any wavelength (λ) is dependent on temperature as described in Eq. 1.

$$I_B(\lambda, T) = \frac{c_1}{\lambda^5\left[exp\left(\frac{c_2}{\lambda T}\right) - 1\right]} \quad (1)$$

In Eq. 1, $c_1 = 2\pi hc^2$ and $c_2 = hc/k$ are the first and second radiation constants, h is Planck's constant, c the speed of light in vacuum, and k the Boltzmann constant. The emission of soot irradiance, I_{soot}, is related to I_B through the emissivity (ε), as shown in Eq. 2. The emissivity of soot ε can be expressed using Hottel and Broughton's empirical relation:

$$I_{soot}(\lambda, T, K, L) = \varepsilon I_B(\lambda, T) = \left[1 - exp\left(-\frac{KL}{\lambda^\alpha}\right)\right] I_B(\lambda, T) \quad (2)$$

The dispersion exponent α in Eq. 2 is dependent on the soot properties and it normally takes a value of 1.39 for visible wavelengths [40,41]. KL is proportional to the amount of soot in the measured spray flame and is normally referred to as the KL factor or as the soot absorption strength [40–46].

As aforementioned, the luminosity of soot from the spray flame ($I_{soot}(\lambda_1)$ and $I_{soot}(\lambda_2)$) was acquired at two different wavelengths (λ_1

Table 1
Thermo-physical properties of Octanal and diesel [a]Obtained from suppliers safety data sheet [26], [b] Obtained from reference [32], [c]Calculated value, [d]Obtained from [33], [e]Obtained from [34], [f]Obtained from [35].

Fuel	Density at atmospheric conditions (kg/m^3)	Lower Calorific Value (LCV) (MJ/kg)	Boiling point (K)	Cetane number	Auto-ignition temperature (K)	Flash-point (K)
Octanal	821[a]	40[c]	444[a]	80[e]	463[e]	325[a]
Diesel (Class A2)	850[b]	43[d]	414–735[a]	53[d]	553[f]	329[a]

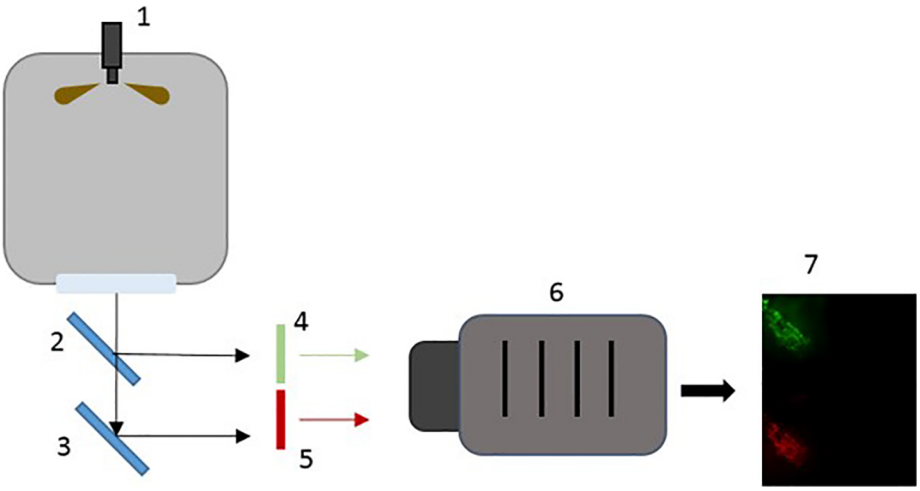

Fig. 2. Simplified experimental set-up schematic including: 1. Injector, 2. 50–50 Beam Splitter, 3. Mirror, 4. 543.5 nm filter, 5. 670 nm filter, 6. High Speed camera and 7. Sample of collected datal.

and λ_2), chosen to be within the camera's optimum spectral response range and also to maximise the change of spectral irradiance with respect to temperature [44,47,48]. The filters were also chosen with a FWHM of 10 nm to avoid a wide pass wavelength range interfering with the accuracy of the calculations. To relate the camera signal (auxiliary units, a.u) with irradiance values, a calibrated tungsten halogen light source was placed in the chamber at the location of the spray and imaged with the camera at different light intensities. From this, the calibration constant relating irradiance to the corresponding camera signal at both wavelengths ($C_{\lambda 1}$ and $C_{\lambda 2}$) was obtained, Eq. 3:

$$I_{soot}(\lambda, T, K, L) = C_{\lambda} S_{\lambda} \quad (3)$$

Once I_{soot} was obtained for both wavelengths, Eq. 2 was solved for T and KL at every pixel location for each of the spray images that were acquired.

The data were processed using an in–house developed Matlab code to obtain the flame temperature and the soot absorption function. As seen in Fig. 2, the optical path length was different for the flame imaged through the red filter than that for the green filter, so spatial alignment was carried out to scale and match the images on a pixel-by-pixel basis. The first step in the spatial alignment process was to separate both green and red flames into two equally sized images. The green flame was then taken as the reference image and the red image was scaled and rotated to match the reference one. The spatially aligned flame images were then isolated from the background, and the calibration parameters obtained using Eq. 3 were applied to convert the pixel's a.u into radiance units. Eq. 2 was then solved numerically for T and KL at every pixel location [40].

The 2C method has some limitations related to its fundamental principles that are detailed in [46,47,49–53], and thus must be treated as a semi-quantitative method. Nonetheless, it is a powerful tool that provides details of the soot and temperature distribution in a flame in a non-intrusive way. Furthermore, in this work, the results for octanal are treated as relative to diesel.

It is noted that in Hottel and Broughton's expression for the emissivity, Eq. 2, the value KL can take is physically limited by the emissivity of a body approaching a black body behaviour, $\varepsilon = 1$. This means that non-blackbody emitters must have a value of $\varepsilon < 1$. Thus, a KL limit must be set based on physical principles and on the wavelengths used, by using Hottel and Broughton's relation for ε and λ (Eq. 2). This resulted in a $KL_{max} = 2.95$ based on a limit $\varepsilon = 0.994$. For $\varepsilon > 0.994$, the KL values cannot be easily resolved and the pixels that become unsolved are set to a $KL_{max} = 2.95$. This results in an underestimation of the soot values, which has also been noted in [46,54,55]. The limiting case where the intensity ratio becomes unsolvable is presented in Fig. 3. Any pixel intensity ratio that lied above the line was rendered as unsolvable and was thus set to a KL value of 2.95.

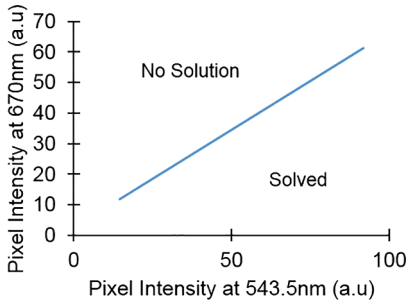

Fig. 3. Line delineating pixel ratios that can be rendered as solved and unsolved.

3. Results and discussion

3.1. Ignition characteristics and soot lift-off length

The ambient temperature of the CVC was significantly higher than the fuel's autoignition temperatures, thus in this work, the CN need not be representative of the ignition delay time. Even though the actual ignition process was not detected through OH* or CH*, the first appearance of soot relative to the start of injection (SoI) was recorded and is referred to as the start of combustion (SoC) throughout the remaining text. In Fig. 4, the x-axis denotes the time from the SoI to the occurrence of various combustion events. All of the event timings are an average of

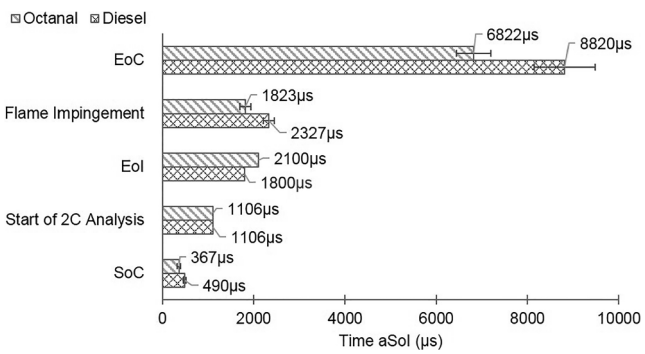

Fig. 4. Timings of various events observed for diesel and octanal.

10 injections except for the start of data analysis, which was manually selected when the signal-to-noise ratio (SNR) was high enough for adequate boundary detection. The start of analysis for T and KL was initiated when the SNR was high enough to extract the flame boundary from the background (at ≈1106 μs); this does not imply that both fuels have the same SoC. The first appearance of soot luminosity (SoC) was observed first for octanal (367 μs) and later on for diesel (490 μs). A T-test was performed, which confirmed that the difference in SoC between the fuels was statistically significant. For both fuels, this first appearance of soot luminosity consisted of small pockets of soot relatively close to the nozzle and at the spray periphery, which then rapidly quenched as the injection proceeded. It is possible that soot-forming conditions were favoured because of the high ambient temperature, rapid evaporation, and rich mixtures in the vicinity of the nozzle during the early SoI. However, these local pockets of soot oxidised fast and were rapidly entrained into the spray core. Evaporative cooling of the fuel could also be causing the quenching of these small pockets of soot by extracting heat from the surroundings.

It was observed that octanal impinged on the wall earlier than diesel,which suggests that combustion proceeded faster for octanal. Furthermore, the end of combustion (EoC) for octanal terminated ≈2000 μs earlier than for diesel, which indicates that oxidation processes proceeded faster for octanal. This faster oxidation could be because of the fuel-bound oxygen in octanal, which reduces the amount of mixing required with ambient oxygen per unit of fuel for a complete burn. In engines, where the temperature decreases soon after the piston moves downwards (after top dead centre), this faster combustion and oxidation would provide soot a better chance to oxidise before the exhaust valve opens, reducing engine-out soot emissions when compared to diesel. Furthermore, the faster combustion and late-stage oxidation can lead to improvements in efficiency, as discussed in [13].

Another parameter that can be used to characterise the combustion properties of a fuel is the flame lift-off length, which is the distance from the nozzle tip to the zone where combustion reactions have stabilised. This will determine the amount of pre-mixing available for a particular fuel and the equivalence ratio at that location, which affects both combustion and emissions [56]. In this work, the soot lift-off length (LoL) was studied, which is the distance between the injector tip and the point at which soot has stabilised, and might not directly correlate with the amount of air entrained upstream. However, other studies have shown that the flame LoL is strongly dependent on the ambient temperature, and that at temperatures above ≈1100 K the difference in flame LoL between fuels becomes small [57,36]. This means that, by setting the ambient temperature in this work to higher values than those reported in the literature, the difference in pre-mixing between both fuels was minimised. It is interesting to note that even though the small local pockets of soot appeared earlier in time for octanal (Fig. 4), the (soot) LoL was further downstream for octanal than for diesel (Fig. 5). This is an initial indicator of its potential as a low sooting fuel, as it is known that the distance from the flame LoL to the soot LoL increases with decreasing sooting propensity of the fuel [58]. Furthermore, this longer soot LoL would also reduce the time available for soot to accumulate and grow, reducing the overall soot.

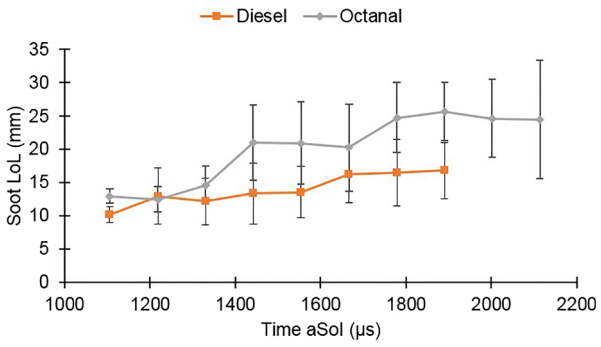

Fig. 5. Soot LoL finishing at the point before the LoL starts decreasing due to the loss of momentum of the fuel at the EoI.

3.2. Spatial distribution of temperature and soot

The temperature and soot spatial distributions of the spray flame for diesel and octanal are presented in Fig. 6 - Fig. 7. These results provided a semi-quantitative understanding of how the soot and temperature profiles developed for both fuels.

The points in time chosen are representative of the start of combustion (1106 μs-1442 μs), the intermediate stages of combustion (2562 μs-3682 μs) and the end of combustion (4802 μs-5362 μs for octanal and 4802 μs-7602 μs for diesel). Fig. 6 presents the spatial distribution of temperature and KL for diesel and Fig. 7 for octanal.

As seen in Fig. 6a and Fig. 7a, after the SoC (1106 μs-1442 μs), both fuels had high and low temperature regions scattered over the entire flame surface, with a noticeably lower flame temperature near the injector tip (top left corner). As the flame developed (2562 μs to 3122 μs for octanal and to 3682 μs for diesel), for both fuels, the localised high temperature regions dispersed, and the temperatures remained fairly constant in the bulk of the flame. Once the flame approached the chamber wall, at ≈1900 μs for octanal and ≈2400 μs for diesel, those parts in contact with the wall had a lower temperature than the rest of the flame due to the transfer of heat to the wall. At a time of ≈3682 μs for octanal, the visible soot accumulated in an area downstream from the injector in an island-like structure. On the other hand, at the same time for diesel, there was still significant soot lingering in the vicinity of the injector. Finally, towards the end of combustion (> 4802 μs), for both fuels, the low temperature regions spread following the wall's curvature and the high temperature regions became smaller and more localised due to the intense air entrainment in the flow recirculation region. It also seems that during the final combustion stages the flame for octanal had a tendency to recoil back onto itself separated from the wall whereas for diesel, the flame remained closer to the wall.

Figs. 6b and 7b show the evolution of the soot distribution for diesel and octanal shortly after the SoC (1106 μs–1442 μs). Overall, diesel produced more soot than octanal. For both fuels, soot initially appeared as scattered patches mostly around the centre of the flame. For diesel, as the flame continued to develop, high soot regions appeared promptly in the flame core and at the tip (2562 μs–3122 μs), as the only oxygen available was at the boundary of the diffusion flame and thus a stronger development of soot was promoted at the flame core. For the same period of time, octanal produced much less soot, and the soot patches with relatively higher values were initially more scattered (2562 μs) and seemed to dissipate more quickly (3122 μs). This shows that during the middle combustion stages, octanal not only produces less soot but also hinders soot growth due to a rapid oxidation.

In view of the similar flame temperatures for both fuels (Fig. 6a and 7a), the differences in soot quantity and distribution were possibly a result of the oxygen content and molecular structure of octanal. The oxygen availability in octanal alters the oxygen equivalence ratio in the spray, and this could have suppressed the formation of soot and enhanced the oxidation of soot that has already formed, due to the formation of O and OH from the combustion of the incoming fuel (discussed in §3.3). This is consistent with the results presented in §3.1, where the longer LoL for octanal implied that there was less time available for soot growth -making it easier to oxidise.

After the EoI, high sooting regions appeared very close to the injector, caused by the burning of the near-nozzle residual vapours and of the fuel expulsions [59]. This was less prominent for octanal than for diesel, due to the fuel-bound oxygen promoting a faster oxidation for octanal. Towards the EoC (> 3682 μs for octanal and > 4802 μs for diesel), a large portion of the flame had impinged on the chamber walls, which caused an increase in soot in the near-wall region as a result of the increased residence time caused by the flame stagnation and the

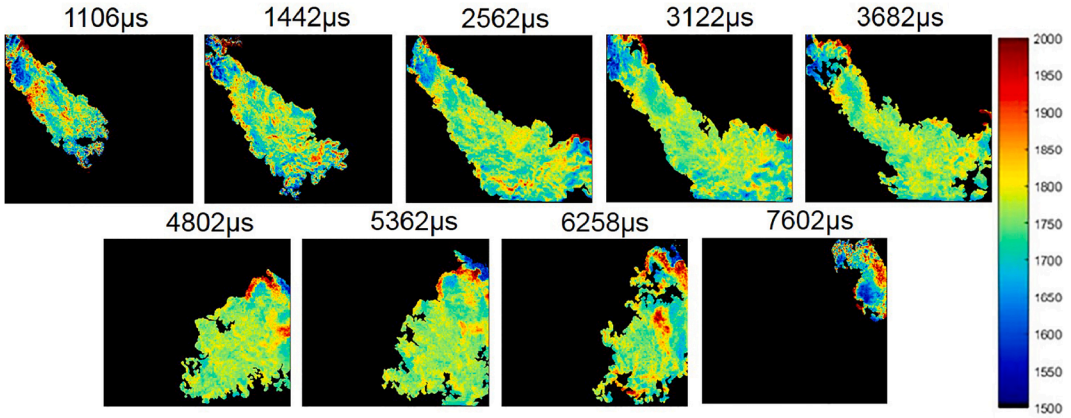

(a) Temperature (K)

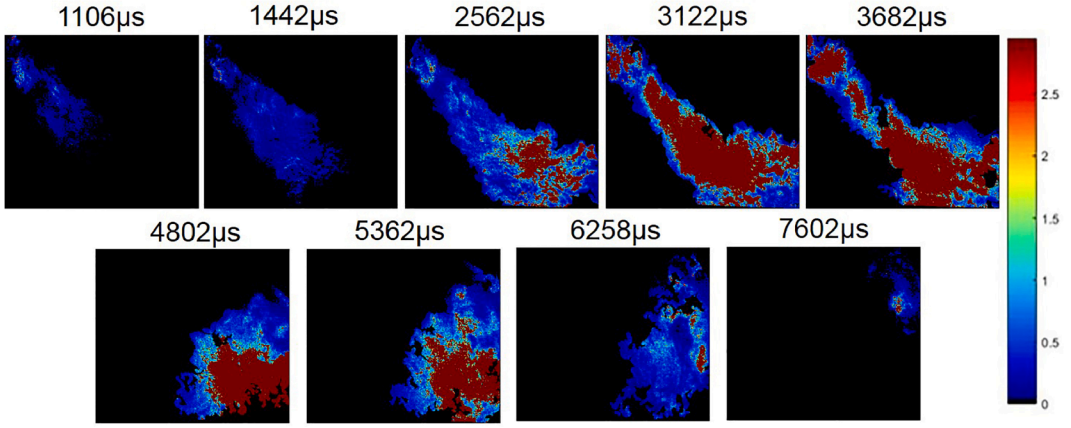

(b) KL

Fig. 6. Diesel spatial distribution, a) Temperature and b) KL.

reduced entrainment of air [60]. For this period, the highly sooting areas were smaller and lower in magnitude for octanal than for diesel. During the final stages of combustion (> 5362 μs) both flames were consumed as the soot mixed with the ambient oxygen and oxidised until combustion terminated. In general, octanal had a lower tendency to soot than diesel, and its high sooting regions were more scattered, dispersed more promptly, and accumulated less at the tip. In addition to studying the spatial distribution of soot and temperature, the percentage of the flame taking different values of soot and temperature was quantitatively characterised. These results are shown in Fig. 8 for diesel and in Fig. 9 for octanal, all as an ensemble average of 10 injection events.

From Fig. 8a and 9a it can be seen that for both fuels, the portion of the flame with a temperature between 1700 K and 1900 K increased as time advanced from 1106 μs to 3682 μs as the flame entrained more hot air and combustion reactions intensified. Towards the EoC, from 4802 μs to 7602 μs, both low temperature (1500 K–1700 K) and high temperature regions (1900 K–2100 K) grew, although the hotter regions experienced a smaller growth. Towards the EoC, as the flame curled due to flame-wall interactions more of it came in contact with the wall, and thus more of it experienced a decrease in temperature. Alongside this increase in area for the lower temperature regions, the percentage of flame area with higher temperature regions (> 1900 K) also increased for both fuels towards the EoC because of the late oxidation stages. This is in accordance with other studies that reported high OH regions surrounding soot clouds and promoting oxidation during the EoC [61]. Overall, the results from Fig. 8a and 9a are in agreement with the ones presented in Fig. 6a and 7a, indicating that the differences in flame temperature between fuels were not significant for the conditions studied except during the of EoC, where a relatively larger percentage of low temperature and high temperature regions were observed for octanal.

The differences in KL distributions between the fuels were larger than those observed for the temperature distributions (Fig. 8b and 9b). Despite these differences, a general trend in soot evolution could be identified: during the SoC (1106 μs–2562 μs), low KL value areas (< 0.4) were observed for most part of the flame; during the intermediate stages of combustion (3682 μs–4802 μs), higher KL value areas (> 0.4) increased in size; and finally, during the EoC (> 4802 μs), low KL value areas increased in size as soot oxidation dominated over soot formation. During the SoC (1106 μs–2562 μs), > 77% of octanal 's flame area had KL values between 0 and 0.2, whereas for diesel, the percentage flame area with this range dropped quickly to 21%. For diesel, at a time of 2562 μs, both a higher and a wider range of KL values developed, where 24% of the flame area had KL values in the range of 0.2–0.4, 15% had KL values in the range of 0.4–0.6 and ≈40% had KL values > 0.6. As combustion proceeded (3682 μs-4802 μs), the regions of high soot grew for both flames, but diesel consistently maintained larger regions of high KL values, whereas nearly 44% of the flame area for octanal remained mostly with KL < 0.4. For diesel, during this period, around 57% of the flame had values of > 2.8, whereas for octanal only 19% of the flame area reached this maximum KL value; even at the peak of the soot formation period, the maximum soot octanal produced was significantly lower than that for diesel. Towards the EoC (> 4802 μs), the high KL value regions decreased in size because most of the soot had oxidised. For octanal this happened faster,

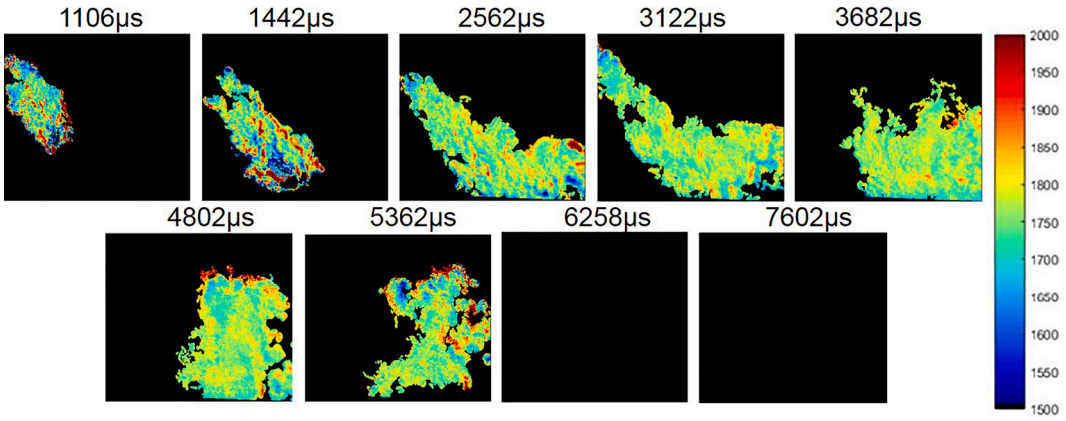

(a) Temperature (K)

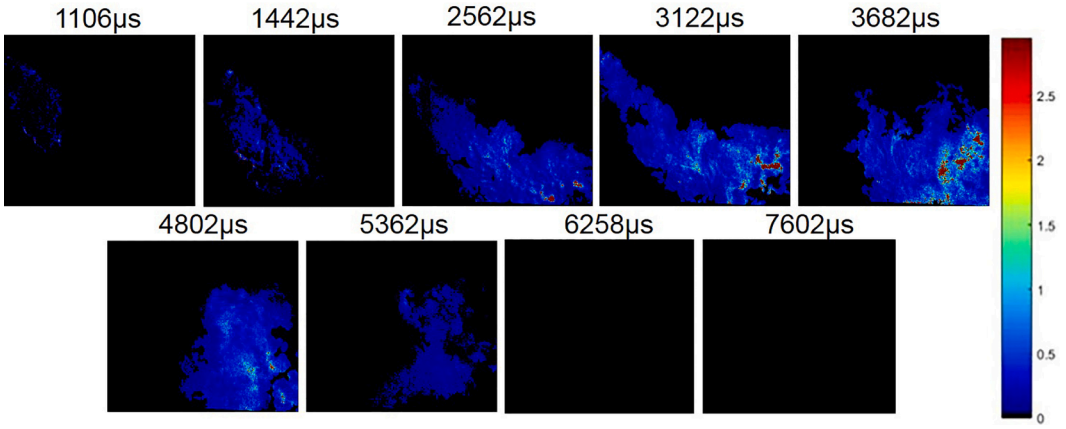

(b) KL

Fig. 7. Octanal spatial distribution, a) Temperature and b) KL.

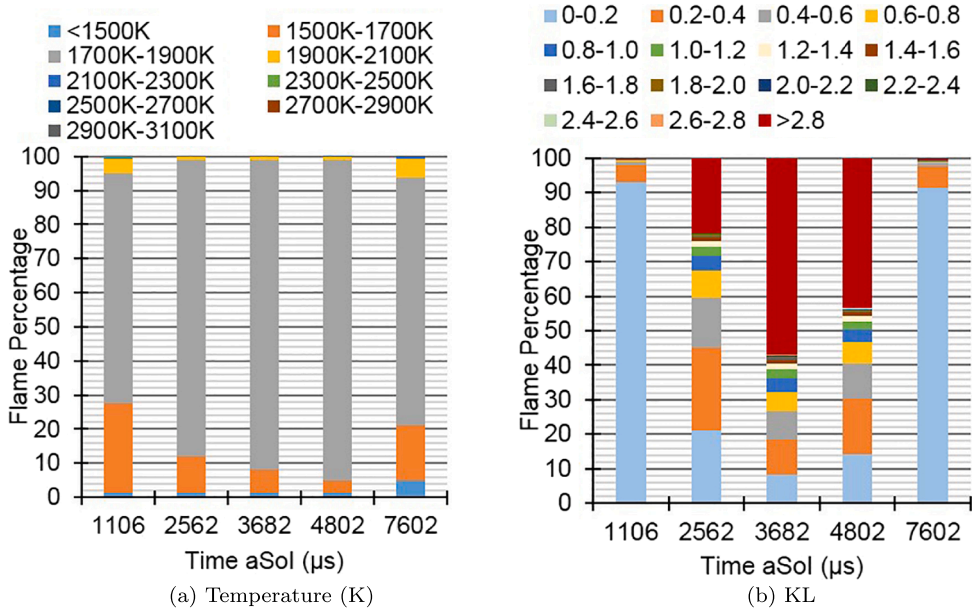

(a) Temperature (K) (b) KL

Fig. 8. Time-resolved diesel distributions for a) Temperature and b) KL.

as by a time of 4802us, 76% of the flame had values of KL < 0.4, whereas for diesel at the same point in time only 30% of the flame area had values of KL < 0.4.

From these results, it is clear that fuelling with neat octanal, when compared to diesel, decreases the maximum soot attained and changes the way in which soot is distributed in the flame. To explore further the soot reduction potential of octanal, the soot temporal evolution was explored.

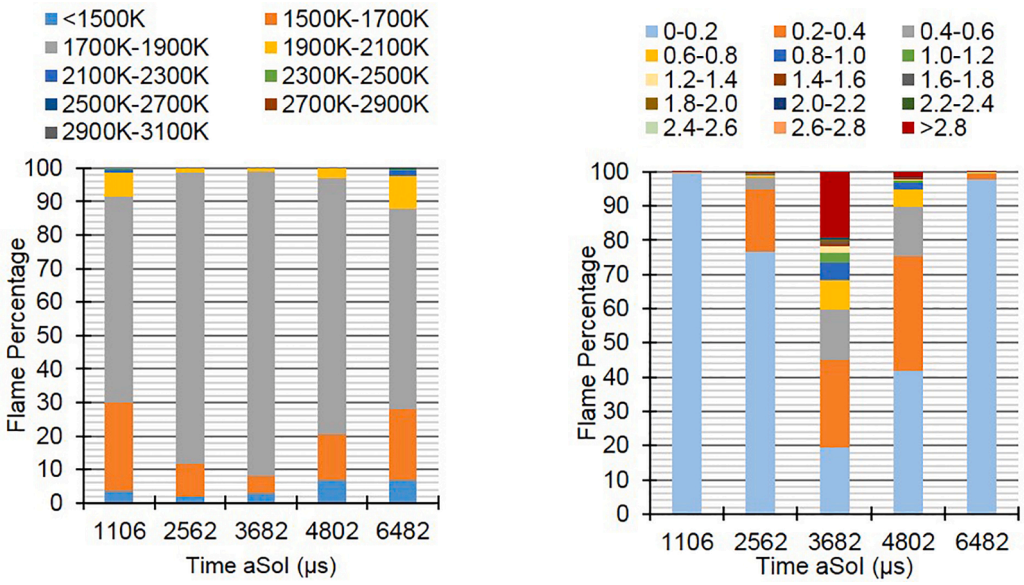

(a) Temperature (K) (b) KL

Fig. 9. Time-resolved octanal distributions for a) Temperature and b) KL.

3.3. Hypotheses on the soot evolution in octanal spray flames

The temporal evolution of soot for both fuels is presented in Fig. 10. The data were obtained by averaging the spatially distributed KL values over the entire flame sampled every 110 μs for each of the 10 injection events. The error bars in the figure cover an uncertainty range of two standard deviations. It can be seen that when compared to diesel, octanal produced less soot throughout the combustion process and had a lower KL peak value. Besides the oxygen content, it has been shown that the chemical structure can affect the sooting propensity of a fuel [20,21,24]. To facilitate the interpretation of the results, the analysis is divided into two stages: the stage dominated by soot formation (positive curve gradient in Fig. 10) and the stage dominated by soot oxidation (negative curve gradient in Fig. 10). By exploring the data presented in Fig. 10 along with literature on the chemical kinetics of aldehydes, preliminary hypotheses have been proposed regarding the soot reduction mechanisms of octanal. It is important to highlight that based on the results discussed in §3.1, the degree of pre-mixing of octanal is expected to be at least equal to that of diesel. Moreover, as the flame temperature was similar for both fuels (§3.2), the results can be treated purely from variations in the chemical structure. The extent of the influence of the fuel structure on soot reduction cannot be fully quantified, as chemical reaction pathways for octanal are not readily available. Thus, the mechanisms described below must be treated as hypotheses.

The first thing to note is that diesel is a complex mixture of different hydrocarbons, mainly aromatics (≈35%), n-alkanes (≈15%), iso-alkanes (≈15%) and cycloalkanes (≈35%) [62], whereas octanal is a linear molecule with a high degree of saturation (Fig. 1). This sets octanal as a low-sooting fuel because the potential for nucleation sites stemming from aromatics and other cyclic structures is reduced when compared to diesel due to the straight chain chemical structure of octanal. It is known that the rate-controlling step in soot formation is the relatively slow formation of the first aromatic ring [63,64]. Thus, fuels which do not readily have ring structures, such as octanal, have a slower production of the first aromatic rings than those fuels that already have ring structures in it [65]. As well as its high degree of linearity, octanal has less amount of C–C bonds than typical diesel components which have higher C-chains, so the sooting propensity of octanal will tend to be lower [66]. In addition to the effects of the carbon backbone chain, the reduction in soot formation could also be attributed to the moiety and oxygen content of octanal. The carbonyl group (C = O) is known to have a higher bond energy than the adjacent bonds, which means that the O atom attached to the carbonyl C atom through a double bond is least likely to participate in soot-forming reactions and instead escape as CO and CO_2 [61,62,66]. In addition to this, the aldehydic H atom is the weakest bond and has the highest reactivity [67–69], so its ease of abstraction could increase the H-atom pool which is known to consume propargyl radicals and in turn hinder the growth of benzenoic rings [6], reducing the soot formation rate.

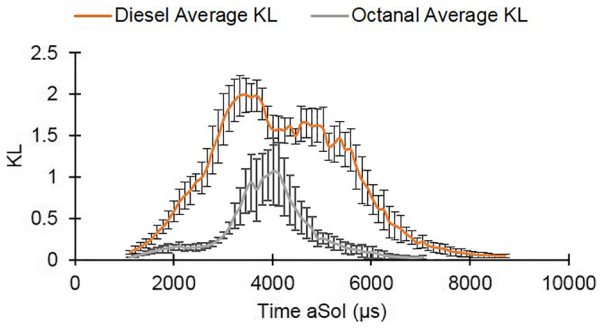

Fig. 10. Temporal evolution of the average KL for diesel and octanal.

Moving on to the soot oxidation rate, it can be seen in Fig. 10 that the soot from the octanal flame took less time to oxidise than for diesel. It is known that soot oxidation processes can happen via break-up of primary soot particles and removal of edge site fragments or via internal burn causing break-up between primary particles [70]. Thus, changes in soot nanostructure that facilitate the above will enhance soot oxidation. Even though little information is available on the oxidation of soot at high temperatures and pressures, and even less is available on the oxidation of aldehydes [70–72], it is known that fuels containing oxygen moieties increase the soot reactivity [73–75]. For octanal, this reactivity could be increased by its fuel-bound oxygen content, which would ultimately increase the surface oxygen content of soot aiding on its oxidation via CO and CO_2 [11]. The increased oxygen content is also known to increase the amorphous character of soot leading to more curved structures, making it more susceptible to oxidative attack [75].

The experimental findings presented in this section have revealed that octanal takes a longer time to form soot and a shorter time to oxidise it. Based on its soot reduction potential and on its similar thermo-physical properties to diesel, it could be a candidate for a drop-in fuel. To what extent any of the mechanisms described hinder soot formation and promote oxidation is not yet clearly understood, and it would be interesting for further investigations to analyse the soot formation and oxidation mechanism of octanal under high pressure and high temperature conditions using computational chemical kinetics.

4. Conclusions

The two-colour pyrometry method was applied to study the combustion process of octanal and diesel in a constant volume chamber that was maintained at a high pressure and temperature to simulate diesel engine-like conditions. In order to study the fuel chemistry effects on the sooting propensity of octanal and diesel, the mixing time was minimised by maintaining the chamber at temperatures much higher than the autoignition temperatures of either fuel. The main findings can be summarised as follows.

The soot lift-off length for octanal was longer than for diesel, which reduced the amount of time that soot had to grow in the flame. Though the same amount of fuel was injected, the combustion of octanal was faster because the fuel-bound oxygen promoted a faster combustion and enhanced soot oxidation.

The spatial distribution of soot for octanal was different to that of diesel, as soot didn't accumulate as much at the core of the spray flame or at the leading edge of the flame during the quasi-steady burn. This was because soot formation was hindered and soot oxidation was enhanced in the jet core due to the fuel-bound oxygen. Towards the end of combustion, soot accumulated at the tip of the flame for both fuels but to a lesser extent for octanal. Despite the variations in the soot distributions, no major differences in the temperature distributions were observed between the fuels.

Octanal produced on average less soot than diesel, as it hindered soot formation and enhanced its oxidation. This was attributed to its non-aromatic content, the effect of fuel-bound oxygen and the chemical implications of the carbonyl group.

Declaration of Competing Interest

The authors declare that they have no known competing financial interests or personal relationships that could have appeared to influence the work reported in this paper.

Acknowledgement

We gratefully acknowledge support from the EPSRC.

References

[1] Bond TC, Doherty SJ, Fahey DW, Forster PM, Berntsen T, Deangelo BJ, et al. Bounding the role of black carbon in the climate system: a scientific assessment. J Geophys Res Atmos 2013;118:5380–552. https://doi.org/10.1002/jgrd.50171.
[2] Booth B, Bellouin N. Black carbon and atmospheric feedbacks. Nature 2015;519:167–8. https://doi.org/10.1038/519167a.
[3] Benajes J, Martín J, García A, Villalta D, Warey A. In-cylinder soot radiation heat transfer in direct-injection diesel engines. Energy Convers Manage 2015;106:414–27. https://doi.org/10.1016/j.enconman.2015.09.059.
[4] Struwe FJ, Foster DE. In-cylinder measurement of particulate radiant heat transfer in a direct injection diesel engine. SAE Technical Papers 2003. https://doi.org/10.4271/2003-01-0072.
[5] Lapuerta M, Rodríguez-Fernández J, Oliva F. Effect of soot accumulation in a diesel particle filter on the combustion process and gaseous emissions. Energy 2012;47:543–52. https://doi.org/10.1016/j.energy.2012.09.054.
[6] McEnally CS, Pfefferle LD, Atakan B, Kohse-Höinghaus K. Studies of aromatic hydrocarbon formation mechanisms in flames: Progress towards closing the fuel gap. Prog Energy Combust Sci 2006;32:247–94. https://doi.org/10.1016/j.pecs.2005.11.003.
[7] Pickett LM, Siebers DL. Soot in diesel fuel jets: effects of ambient temperature, ambient density, and injection pressure. Combust Flame 2004;138:114–35. https://doi.org/10.1016/j.combustflame.2004.04.006.
[8] Glassman I. Combustion. Academic Press, Inc; 1977.
[9] Gonzalez MA, Piel W, Asmus T, Clark W, Garbak J, Liney E, et al. Oxygenates screening for advanced petroleum-based diesel fuels: Part 2. The effect of oxygenate blending compounds on exhaust emissions. SAE Trans 2001;110:2246–55. https://doi.org/10.4271/2001-01-3632.
[10] Härtl M, Seidenspinner P, Jacob E, Wachtmeister G. Oxygenate screening on a heavy-duty diesel engine and emission characteristics of highly oxygenated oxymethylene ether fuel OME1. Fuel 2015;153:328–35. https://doi.org/10.1016/j.fuel.2015.03.012.
[11] Guerrero Peña GD, Hammid YA, Raj A, Stephen S, Anjana T, Balasubramanian V. On the characteristics and reactivity of soot particles from ethanol-gasoline and 2,5-dimethylfuran-gasoline blends. Fuel 2018;222:42–55. https://doi.org/10.1016/j.fuel.2018.02.147.
[12] Das DD, St. John PC, McEnally CS, Kim S, Pfefferle LD. Measuring and predicting sooting tendencies of oxygenates, alkanes, alkenes, cycloalkanes, and aromatics on a unified scale. Combust Flame 2018;190:349–64. https://doi.org/10.1016/j.combustflame.2017.12.005.
[13] Dam N, Willems R, Wakefield C, Bakker P, Somers B, Brewer M, et al. Investigation of late stage conventional diesel combustion – effect of additives. SAE Technical Paper Series 2018;1:1–6. https://doi.org/10.4271/2018-01-1787.
[14] Das DD, McEnally CS, Pfefferle LD. Sooting tendencies of unsaturated esters in nonpremixed flames. Combust Flame 2015;162:1489–97. https://doi.org/10.1016/j.combustflame.2014.11.012.
[15] Park W, Park S, Reitz RD, Kurtz E. The effect of oxygenated fuel properties on diesel spray combustion and soot formation. Combust Flame 2017;180:276–83. https://doi.org/10.1016/j.combustflame.2016.02.026.
[16] Kerschgens B, Cai L, Pitsch H, Heuser B, Pischinger S. Di-n-buthylether, n-octanol, and n-octane as fuel candidates for diesel engine combustion. Combust Flame 2016;163:66–78. https://doi.org/10.1016/j.combustflame.2015.09.001.
[17] Liu H, Li S, Zheng Z, Xu J, Yao M. Effects of n-butanol, 2-butanol, and methyl octynoate addition to diesel fuel on combustion and emissions over a wide range of exhaust gas recirculation (EGR) rates. Appl Energy 2013;112:246–56. https://doi.org/10.1016/j.apenergy.2013.06.023.
[18] Song H, Peng Z, Quinton KS, Zhao H, Ladommatos N. An experimental study on effects of fuel oxygenates on diesel engine combustion. Energy Procedia 2015;66:17–20. https://doi.org/10.1016/j.egypro.2015.02.009.
[19] Tran LS, Sirjean B, Glaude PA, Fournet R, Battin-Leclerc F. Progress in detailed kinetic modeling of the combustion of oxygenated components of biofuels. Energy 2012;43:4–18. https://doi.org/10.1016/j.energy.2011.11.013.
[20] Lemaire R, Lapalme D, Seers P. Analysis of the sooting propensity of C-4 and C-5 oxygenates: comparison of sooting indexes issued from laser-based experiments and group additivity approaches. Combust Flame 2015;162:3140–55. https://doi.org/10.1016/j.combustflame.2015.03.018.
[21] Zhou L, Dam NJ, Boot MD, de Goey LP. Investigation of the effect of molecular structure on sooting tendency in laminar diffusion flames at elevated pressure. Combust Flame 2014;161:2669–77. https://doi.org/10.1016/j.combustflame.2014.04.009.
[22] Köhler M, Kathrotia T, Oßwald P, Fischer-Tammer ML, Moshammer K, Riedel U. 1-, 2- and 3-Pentanol combustion in laminar hydrogen flames – a comparative experimental and modeling study. Combust Flame 2015;162:3197–209. https://doi.org/10.1016/j.combustflame.2015.05.007.
[23] Heuser B, Laible T, Jakob M, Kremer F, Pischinger S. C8-Oxygenates for clean diesel combustion. SAE Int 2014. https://doi.org/10.4271/2014-01-1253.
[24] Pepiot-Desjardins P, Pitsch H, Malhotra R, Kirby SR, Boehman AL. Structural group analysis for soot reduction tendency of oxygenated fuels. Combust Flame 2008;154:191–205. https://doi.org/10.1016/j.combustflame.2008.03.017.
[25] Hong Z, Davidson DF, Vasu SS, Hanson RK. The effect of oxygenates on soot formation in rich heptane mixtures: a shock tube study. Fuel 2009;88:1901–6. https://doi.org/10.1016/j.fuel.2009.04.013.
[26] SDS Octanal, CAS 124-13-0; 2013.
[27] Kamm B, Gruber P, Kamm M. Ullmann's Encyclopedia of Industrial Chemistry; 2000.
[28] Shi R, Wang F, Mu X, Li Y, Huang X, Shen W. MgO-supported Cu nanoparticles for efficient transfer dehydrogenation of primary aliphatic alcohols. Catal Commun 2009;11:306–9. https://doi.org/10.1016/j.catcom.2009.10.023.
[29] Julis J, Leitner W. Synthesis of 1-octanol and 1,1-dioctyl ether from biomass-derived platform chemicals. Angewandte Chemie – International Edition 2012;51:8615–9. https://doi.org/10.1002/anie.201203669.
[30] Kajaste R. Chemicals from biomass – managing greenhouse gas emissions in biorefinery production chains – a review. J Clean Prod 2014;75:1–10. https://doi.org/10.1016/j.jclepro.2014.03.070.
[31] Kunjapur AM, Prather KL. Microbial engineering for aldehyde synthesis. Appl Environ Microbiol 2015;81:1892–901. https://doi.org/10.1128/AEM.03319-14.
[32] Hydrocarbons Jones J. Physical properties and their relevance to utilisation. Ventus Publishing ApS; 2010.
[33] Song H, Quinton K, Peng Z, Zhao H, Ladommatos N. Effects of oxygen content of fuels on combustion and emissions of diesel engines. Energies 2016;9:28. https://doi.org/10.3390/en9010028.
[34] Harnisch F, Blei I, Santos TRD, Möller M, Nilges P, Eilts P, et al. From the test-tube to the test-engine: assessing the suitability of prospective liquid biofuel compounds. RSC Adv 2013;3:9594–605. https://doi.org/10.1039/c3ra40354h.
[35] Patro TN, Larue DA. Alternate fueled powertrain – an insight into its combustion related NVH issues. SAE Technical 1999. 10.4271/1999-01-1758.
[36] Pickett LM, Siebers DL. Fuel effects on soot processes of fuel hets at DI diesel

conditions. SAE International 2003. https://doi.org/10.4271/2003-01-3080.
[37] Manin J, Pickett LM, Skeen SA. Two-color diffused back-illumination imaging as a diagnostic for time-resolved soot measurements in reacting sprays. SAE Int J Engines 2013;6. https://doi.org/10.4271/2013-01-2548. 2013–01-2548.
[38] Sison K, Ladommatos N, Song H, Zhao H. Soot generation of diesel fuels with substantial amounts of oxygen-bearing compounds added. Fuel 2007;86(3):345–52. https://doi.org/10.1016/j.fuel.2006.07.019.
[39] Pos R, Avulapati M, Wardle R, Cracknell R, Megaritis T, Ganippa L. Combustion of ligaments and droplets expelled after the end of injection in a multi-hole diesel injector. Fuel 2017;197:459–66. https://doi.org/10.1016/j.fuel.2017.02.048.
[40] Hottel HC, Broughton FP. Determination of true temperature and total radiation from luminous gas flames. Ind Eng Chem Anal Edition 1932;4:166–75. https://doi.org/10.1021/ac50078a004.
[41] Matsui Y, Kamimoto T, Matsuoka S. Formation and oxidation processes of soot particulates in a D.I. diesel engine – an experimental study via the two-color method. SAE International 1982.
[42] Singh S, Reitz RD, Musculus MPB. 2-Color thermometry experiments and high-speed imaging of multi-mode diesel engine combustion. SAE Technical 2005. 10.4271/2005-01-3842.
[43] Vögelin P, Obrecht P, Boulouchos K. Experimental investigation of multi-in-cylinder pyrometer measurements and exhaust soot emissions under steady and transient operation of a heavy-duty diesel engine. SAE Int J Engines 2013;6:1855–65. https://doi.org/10.4271/2013-24-0177.
[44] Matsui Y, Kamimoto T, Matsuoka S. A study on the time and space resolved measurement of flame temperature and soot concentration in a D.I. diesel engine by the two-color method. SAE International 1979.
[45] Hampson GJ, Reitz RD. Two-color imaging of in-cylinder soot concentration and temperature in a heavy-duty DI diesel engine with comparison to multidimensional modeling for single and split injections. SAE Technical 1998. https://doi.org/10.4271/980524.
[46] Payri F, Pastor JV, García JM, Pastor JM. Contribution to the application of two-colour imaging to diesel combustion. Meas Sci Technol 2007;18:2579–98. https://doi.org/10.1088/0957-0233/18/8/034.
[47] Ladommatos N, Zhao H. A guide to measurement of flame temperature and soot concentration in diesel engines using the two-colour method part II: implementation. SAE Technical Paper 1994. https://doi.org/10.4271/941956.
[48] Huang Y, Yan Y, Riley G. Vision-based measurement of temperature distribution in a 500-kW model furnace using the two-colour method. Meas: J Int Meas Confederation 2000;28:175–83. https://doi.org/10.1016/S0263-2241(00)00010-5.
[49] Ladommatos N, Zhao H. A guide to measurement of flame temperature and soot concentration in diesel engines using the two-colour method part I: principles. SAE Technical Paper 1994. https://doi.org/10.4271/941956.
[50] Musculus MP, Singh S, Reitz RD. Gradient effects on two-color soot optical pyrometry in a heavy-duty DI diesel engine. Combust Flame 2008;153:216–27. https://doi.org/10.1016/j.combustflame.2007.10.023.
[51] Zhang J, Jing W, Roberts WL, Fang T. Soot measurements for diesel and biodiesel spray combustion under high temperature highly diluted ambient conditions. Fuel 2014;135:340–51. https://doi.org/10.1016/j.fuel.2014.06.071.
[52] Di Stasio S, Massoli P. Influence of the soot property uncertainties in temperature and volume-fraction measurements by two-colour pyrometry. Meas Sci Technol 1994;5:1453–65. https://doi.org/10.1088/0957-0233/5/12/006.
[53] Braun A, Shah N, Huggins FE, Kelly KE, Sarofim A, Jacobsen C, et al. X-ray scattering and spectroscopy studies on diesel soot from oxygenated fuel under various engine load conditions. Carbon 2005;43:2588–99. https://doi.org/10.1016/j.carbon.2005.05.017.
[54] Bakenhus M, Reitz RD. Two-color combustion visualization of single and split injections in a single-cylinder heavy-duty D.I. diesel engine using an endoscope-based imaging system. SAE Technical 1999. 10.4271/1999-01-1112.
[55] Svensson KI, Mackrory AJ, Richards MJ, Tree DR. Calibration of an RGB, CCD camera and interpretation of its two-color images for KL and temperature. SAE Technical 2005. https://doi.org/10.4271/2005-01-0648.
[56] Pickett LM, Siebers DL, Idicheria CA. Relationship between ignition processes and the lift-off length of diesel fuel jets. SAE Technical 2005. https://doi.org/10.4271/2005-01-3843.
[57] Mueller CJ, Pitz WJ, Pickett LM, Martin GC, Siebers DL, Westbrook CK. Effects of oxygenates on soot processes in DI diesel engines: experiments and numerical simulations. SAE International 2003. https://doi.org/10.4271/2003-01-1791.
[58] Pickett LM, Siebers DL. Soot formation in diesel fuel jets near the lift-off length. Int J Engine Res 2006;7:103–30. https://doi.org/10.1243/146808705X57793.
[59] Pos R, Ganippa L. Characteristics of high pressure diesel sprays at the end of injection. IMechE ICE 2015.
[60] Liu Y, Li J, Jin C. Fuel spray and combustion characteristics of butanol blends in a constant volume combustion chamber. Energy Convers Manage 2015;105:1059–69. https://doi.org/10.1016/j.enconman.2015.08.047.
[61] Dec JE, Tree DR. Diffusion-flame/wall interactions in a heavy-duty DI diesel engine. SAE Technical 2001. https://doi.org/10.4271/2001-01-1295.
[62] Pitz WJ, Mueller CJ. Recent progress in the development of diesel surrogate fuels. Prog Energy Combust Sci 2011;37:330–50. https://doi.org/10.1016/j.pecs.2010.06.004.
[63] Tree DR, Svensson KI. Soot processes in compression ignition engines. Prog Energy Combust Sci 2007;33:272–309. https://doi.org/10.1016/j.pecs.2006.03.002.
[64] Glassman I. Soot formation in combustion processes. Symp (Int) Combust 1989;22:295–311. https://doi.org/10.1016/S0082-0784(89)80036-0.
[65] Ladommatos N, Rubenstein P, Bennett P. Some effects of molecular structure of single hydrocarbons on sooting tendency. Fuel 1996;75:114–24. https://doi.org/10.1016/0016-2361(94)00251-7.
[66] Ogawa H, Miyamoto N, Yagi M. Chemical-kinetic analysis on PAH formation mechanisms of oxygenated fuels. SAE Technical 2003. https://doi.org/10.4271/2003-01-3190.
[67] Zhang J, Pan L, Mo J, Gong J, Huang Z, Law CKA. shock tube and kinetic modeling study of n-butanal oxidation. Combust Flame 2013;160:1541–9. https://doi.org/10.1016/j.combustflame.2013.04.002.
[68] DaSilva G, Bozzelli J. Enthalpies of formation, bond dissociation energies, and molecular structures of the n-aldehydes (acetaldehyde, propanal, butanal, pentanal, hexanal, heptanal) and their radicals. J Phys Chem 2006;110:13058–67.
[69] Pelucchi M, Ranzi E, Frassoldati A, Faravelli T. Alkyl radicals rule the low temperature oxidation of long chain aldehydes. Proc Combust Inst 2017;36:393–401. https://doi.org/10.1016/j.proci.2016.05.051.
[70] Ghiassi H, Toth P, Jaramillo IC, Lighty JAS. Soot oxidation-induced fragmentation: part 1: the relationship between soot nanostructure and oxidation-induced fragmentation. Combust Flame 2016;163:179–87. https://doi.org/10.1016/j.combustflame.2015.09.023.
[71] Jaramillo IC, Gaddam CK, Vander Wal RL, Huang CH, Levinthal JD, Lighty JAS. Soot oxidation kinetics under pressurized conditions. Combust Flame 2014;161:2951–65. https://doi.org/10.1016/j.combustflame.2014.04.016.
[72] Pelucchi M, Cavallotti C, Ranzi E, Frassoldati A, Faravelli T. Relative reactivity of oxygenated fuels: alcohols, aldehydes, ketones, and methyl esters. Energy Fuels 2016;30:8665–79. https://doi.org/10.1021/acs.energyfuels.6b01171.
[73] Vander Wal RL, Mueller CJ. Initial investigation of effects of fuel oxygenation on nanostructure of soot from a direct-injection diesel engine. Energy Fuels 2006;20:2364–9. https://doi.org/10.1021/ef060201+.
[74] Abboud J, Schobing J, Legros G, Matynia A, Bonnety J, Tschamber V, et al. Impacts of ester's carbon chain length and concentration on sooting propensities and soot oxidative reactivity: Application to Diesel and Biodiesel surrogates. Fuel 2018;222:586–98. https://doi.org/10.1016/j.fuel.2018.02.103.
[75] Serhan N, Tsolakis A, Martos FJ. Effect of propylene glycol ether fuelling on the different physico-chemical properties of the emitted particulate matters: Implications of the soot reactivity. Fuel 2018;219:1–11. https://doi.org/10.1016/j.fuel.2018.01.065.